Final Draft
Manuscript available at: https://doi.org/10.1061/(ASCE)ST.1943-541X.0001965
Full citation: Gerbo, EJ, Wang, Y, Tumbeva, MD, Thrall,* AP, Smith, BJ, and Zoli, TP (2018) "Behavior of an Adjustable Bolted Steel Plate Connection during Field Installation." Journal of Structural Engineering, 144(3), 04017223

Behavior of an Adjustable Bolted Steel Plate Connection during Field Installation

Evan J. Gerbo, S.M.ASCE[1]; Yao Wang, S.M.ASCE[2]; Mirela D. Tumbeva, S.M.ASCE[3]; Ashley P. Thrall, A.M.ASCE[4]; Brian J. Smith, P.E.[5]; Theodore P. Zoli, P.E., M.ASCE[6]

ABSTRACT

This paper presents a bolted steel plate connection to join steel members at a range of angles with the capability of adjusting in-situ to accommodate additional angles or tolerances through cold bending. The connection features plates that are pre-bent (cold bent via a press brake) to defined angles, and then further cold bent during field installation (by bolt tightening) until turn-of-nut criteria are met. This approach uses a small number of unique components to facilitate prefabrication and rapid erection. Geometric studies were performed to select connection parameters for greatest adaptability to manufacturing/erection tolerances and versatility of member dimensions. A total of 13 scenarios were tested under field installation conditions to investigate the effect of the (1) bolt tightening procedure, (2) amount and direction of field bending, and (3) plate angle on surface strains. Strains were measured using Digital Image Correlation - an optical technique that captures full-field data. This paper presents a novel approach for bolted steel connections, measures the impact of field installation on surface strains, and makes implementation and design recommendations.

[1]Graduate Student, Kinetic Structures Laboratory, Department of Civil and Environmental Engineering and Earth Sciences, University of Notre Dame, Notre Dame, IN 46556. E-mail: egerbo@nd.edu

[2]Graduate Student, Kinetic Structures Laboratory, Department of Civil and Environmental Engineering and Earth Sciences, University of Notre Dame, Notre Dame, IN 46556. E-mail: ywang32@nd.edu

[3]Graduate Student, Kinetic Structures Laboratory, Department of Civil and Environmental Engineering and Earth Sciences, University of Notre Dame, Notre Dame, IN 46556. E-mail: mtumbeva@nd.edu

[4]Myron and Rosemary Noble Assistant Professor of Structural Engineering, Kinetic Structures Laboratory, Department of Civil and Environmental Engineering and Earth Sciences, University of Notre Dame, Notre Dame, IN 46556. (corresponding author) E-mail: athrall@nd.edu

[5]Assistant Teaching Professor and Research Engineer, Kinetic Structures Laboratory, Department of Civil and Environmental Engineering and Earth Sciences, University of Notre Dame, 228 Cushing Hall, Notre Dame, IN 46556. E-mail: bsmith24@nd.edu

[6]National Bridge Chief Engineer, HNTB Corporation, Empire State Building, 350 5th Ave., 57th Floor, New York, NY 10118. E-mail: tzoli@hntb.com

Author Keywords: Bolted steel connection; Cold bending; Prefabrication; Rapid erection; Digital Image Correlation

INTRODUCTION

This paper presents a novel approach for rapid erection of steel structures using prefabricated, bolted connections that form moment-resisting joints between structural members in double shear at a range of angles. The connection is adjustable, meaning that it is capable of changing angle in-situ to accommodate additional angles or manufacturing and erection tolerances. More specifically, connection plates are prefabricated by cold bending (via a press brake) to specific angles forming a kit-of-parts comprised of a small number of unique components that can be used for a wide variety of structural systems. For a given structure, these plates are then further cold bent during field installation (via bolt tightening) until turn-of-nut criteria are met. Figure 1 shows a connection between wide flange sections. Advantages of this approach include reduced cost and construction time as prefabricated components can be used to form a wide variety of angled connections while also allowing for erection tolerances. This approach can be implemented for any moment-resisting joint between angled structural members in buildings (*e.g.*, apex connections of portal frames) and bridges (*e.g.*, angled connections of arch and truss bridges). This is the first investigation of cold bending for a kit-of-parts adjustable steel connection. The focus of this paper is on the geometric development of the connection and measuring the surface strains induced during field installation. This research is undertaken for a connection between flanges of wide flange structural members, but other connection orientations/section shapes are possible. In addition to the development of the adjustable connections, this research is relevant to double shear connections using cold bent plates in general and is useful in assessing their behavior, as well as setting bend tolerances for fabrication.

Cold bending is an appealing strategy to achieve adjustability as it offers cost and time savings, as opposed to heat-assisted bending (FHWA, 2015c), and can be readily performed in the field. The implementation of cold bending for thin structural sections is well established in the building industry, including implementations as early as the 1850s and design standards dating from 1946 (Yu et al., 1996). However, applications are typically limited to structural members (Yu and LaBoube, 1997; Davies, 2000; Hancock, 2003) with research involving connections primarily focused on thin-walled fastener connections (Yu and LaBoube, 1997; Hancock, 2003), in addition to bolted lap splices and a few other types (Chung and Lau, 1999; Pedreschi et al., 1997). Cold bending (for bend radii exceeding $5t$, where t is the thickness) has only been permitted in the bridge industry since a 2012 code revision, based on the findings of a Texas Department of Transportation study (Keating and Christian, 2012; AASHTO, 2012). Cold bending has been used in bridges including dapped girders (Keating and Christian, 2012; TXDOT, 2015), curved girder bridges (Gergess and Sen, 2005a,b, 2008, 2009), a gussetless truss bridge (Cota and Zoli, 2012), and connections for large skew bridges (HNTB Corporation, Genesis Structures, Inc., Structural Engineering Associates, Iowa State University, 2014).

The primary benefit of this type of connection is adjustability, both in terms of connecting members at different angles and accommodating manufacturing/erection tolerances. In conventional arch or truss bridges, these connections could join angled members, thereby avoiding gusset plates [*e.g.*, gussetless truss bridge (Cota and Zoli, 2012)]. Further, these connections could be featured in modular bridges [*e.g.*, Pratt truss or network tied arch concepts proposed in Gerbo et al. (2016a)] to reduce construction time. In a building environment, these connections could join members of steel portal frames. The power of the connection lies in the kit-of-parts approach which can be used for a wide variety of structural components.

OBJECTIVES AND SCOPE

The objective of this research is to develop a versatile adjustable bolted steel plate connection and to investigate the behavior of this connection during field installation. A geometric investigation of the adjustable plate connection was performed to select parameters for manufacturing and erection tolerances as well as versatility of member dimensions. The authors have previously investigated the behavior of the connection during the prefabrication process (Gerbo et al., 2016b). In this prior work, full-field three-dimensional (3D) residual surface strains induced during cold bending (via a press brake) were measured using Digital Image Correlation (DIC) and compared with finite element predictions. The research presented in this paper focuses on the surface strains induced in the connection during field installation (*i.e.*, cold bending via bolt tightening). A total of 13 scenarios were tested under field installation conditions, with full-field 3D surface strains measured using DIC, to investigate the effect of the (1) bolt tightening procedure, (2) amount and direction of field bending, and (3) plate angle on surface strains. This paper develops a novel concept for an adjustable bolted steel plate connection, measures surfaces strains induced during field installation, and makes recommendations for design and implementation.

GEOMETRIC INVESTIGATION OF CONNECTION PARAMETERS

An extensive investigation to determine optimal geometric parameters (*e.g.*, plate length, initial plate angles, bend radii, bolt hole type, member flange thickness, member depth, and connection angle) was performed. Throughout this paper, the term "plate" refers to the plate connectors between the members. These plates connect flanges of members, which are referred to as simply "member."

Geometric Parameters

The adjustable connection is defined by the geometric parameters in Table 1 and shown in Figure 2. For this study, the top and bottom plates are assumed to be identical (aside from their width). However, the equations provided are expressed in general terms such that a designer could choose different length, angle, and radii of curvature of the top and bottom plates (note that the thickness and hole spacing are assumed to be the same in the top and bottom plate).

The pre-bent top and bottom plate angles (γ = β) are chosen to join a range of shallow angled connections. The member angle (α) is considered for ranges of up to 5° greater than or less than the pre-bent plate angles. A variety of top and bottom plate lengths (l_1 = l_2) and two different radii of curvature for the top and bottom plates (r_t = r_b) were investigated. The plate thickness (t_s) is selected to be on the order of half of the member flange thickness (t_m) for the considered standard rolled wide flange members (W8, W10, and W12) with depths, d_m. This is an appropriate proportion for the proposed double-shear connection. The hole sizes in the member (d_{mh}) are the maximum allowable hole sizes for oversize, short slot, and long slot types for the selected bolt diameter (d_b) per design code (AASHTO, 2014). Only oversized holes are considered for the holes in the plate (d_{ph}) as it will be in direct contact with the bolt head and nut. Oversized, short or long slots are necessary for the bolt up procedure. Note that the use of slotted holes in girder splice type connections is not currently allowed by Code (AASHTO, 2014). This research does not address the effect of hole size on the ultimate strength of the connection, and this will be the focus of future work. The end distance between the bolt hole centerline and the edge of the plate (l_3) and the edge of the member (l_4) is held constant. This is chosen to be more than the minimum edge distance and less than the maximum edge distance prescribed by Code (AASHTO, 2014).

A study was performed to determine an optimized combination of the parameters. The parameters investigated include the plate lengths (l_1 = l_2), initial plate angles (γ = β), plate radii of curvature (r_t = r_b), member slot type (d_{mh}), member thickness (t_m), member depth (d_m), and connection angle (α) using the values provided in Table 1. The following sections first define feasibility of a combination of parameters and then discuss the parametric investigation.

Determining Feasibility of a Combination of Geometric Parameters

A feasible combination of geometric parameters is defined as one for which a bolt can pass through holes in the top plate, member, and bottom plate (*i.e.*, no interference between the bolt and locations A-L in Figure 2D). To determine its feasibility, a comprehensive search of bolt locations was performed for all angles and lateral positions of the bolt. Starting with the bolt in a vertical orientation (*i.e.*, parallel to connection centerline) and centered on the member hole, the clearances between the bolt and locations A-L were calculated. The angular orientations range from where the bolt is parallel to the member in either direction (a range of 180^o in increments of 1^o). All lateral locations of the bolt are considered from the furthest left to the furthest right of locations A-L [in increments of 0.397 mm (0.0156 in.)].

Bolt clearances were determined by calculating the coordinates of locations A-L. Then, the amount of clearance (c) between the location and the bolt is:

$$c = |\vec{v}| \sin(\omega) \tag{1}$$

where $\vec{v}$ is the vector from the bolt edge line ($\vec{u}$) to the location, and ω is the angle between these vectors which can be found as follows:

$$\omega = \sin^{-1}\left(\frac{\vec{u}\times\vec{v}}{|\vec{u}||\vec{v}|}\right) \tag{2}$$

The clearance is calculated for locations A-L (equations provided in the following sub-section). Note that on the left side of the bolt $\vec{u}$ is drawn pointing upward, and on the right side of the bolt $\vec{u}$ is drawn pointing downward. A positive value of c indicates available clearance and a negative value represents lack of clearance (*i.e.*, interference) between the bolt and plates.

Equations for Locations of Interference

Equations for locations A-L are provided below, with subscripts x referring to the horizontal coordinate and y to the vertical coordinate with respect to the origin in Figure 2. All variables are defined in Table 1 and Figure 2. Angles in the equations are in units of radians and should be less than $\pi/2$. The equations shown here are for the top flange of the member, on the right side of the centerline. Analogous equations are used for the other locations.

The coordinates of locations A-D on the top plate are as follows:

$$\begin{aligned}
A_x &= l_5\cos\gamma + \frac{t_s}{2}\sin\gamma - \frac{d_{ph}}{2}\cos\gamma; \quad A_y = -\left(l_5 - \frac{t_s}{2}\tan\gamma\right)\sin\gamma + t_s\cos\gamma + v_1 + \frac{d_{ph}}{2}\sin\gamma \\
B_x &= l_5\cos\gamma + \frac{t_s}{2}\sin\gamma + \frac{d_{ph}}{2}\cos\gamma; \quad B_y = -\left(l_5 - \frac{t_s}{2}\tan\gamma\right)\sin\gamma + t_s\cos\gamma + v_1 - \frac{d_{ph}}{2}\sin\gamma \\
C_x &= l_5\cos\gamma - \frac{t_s}{2}\sin\gamma - \frac{d_{ph}}{2}\cos\gamma; \quad C_y = -\left(l_5 - \frac{t_s}{2}\tan\gamma\right)\sin\gamma + v_1 + \frac{d_{ph}}{2}\sin\gamma \\
D_x &= l_5\cos\gamma - \frac{t_s}{2}\sin\gamma + \frac{d_{ph}}{2}\cos\gamma; \quad D_y = -\left(l_5 - \frac{t_s}{2}\tan\gamma\right)\sin\gamma + v_1 - \frac{d_{ph}}{2}\sin\gamma
\end{aligned} \tag{3}$$

where l_5 is the distance from the centerline to the top plate hole along the plate axis:

$$l_5 = \left(\frac{l_1}{2} - l_3\right) + \left(r_t + \frac{t_s}{2}\right)(\tan\gamma - \gamma) \tag{4}$$

Length v_1 is measured from the origin to the extension of the plate as drawn. This is different for each contact type (Figure 2E) for the top plate (T):

$$\begin{aligned}&\text{Type T1 if: } \alpha \geq \gamma \text{ and } r_t \sin\gamma \geq g\\&\text{Type T2 if: } \alpha \geq \gamma \text{ and } r_t \sin\gamma < g\\&\text{Type T3 if: } \alpha < \gamma\end{aligned} \tag{5}$$

Length v_1 can be found as:

$$v_1 = \left\{\begin{matrix} (r_t \sin\gamma)\tan\gamma - r_t \cos\left(\sin^{-1}(\frac{g}{r_t})\right) - \cos\gamma & \text{if T1} \\ g\tan\gamma & \text{if T2} \\ r_t \sin\gamma \tan\gamma + v_2 - (r_t \sin\gamma + h_1 - g)\tan\alpha & \text{if T3} \end{matrix}\right\} \tag{6}$$

where the vertical (v_2) and horizontal (h_1) dimensions of the straight portion of the top plate are:

$$v_2 = \left[\frac{l_1}{2} + \left(r_t + \frac{t_s}{2}\right)(\tan\gamma - \gamma) - \tan\gamma\left(r_t + \frac{t_s}{2}\right)\right]\sin\gamma \tag{7}$$

$$h_1 = \left[\frac{l_1}{2} + \left(r_t + \frac{t_s}{2}\right)(\tan\gamma - \gamma) - \tan\gamma\left(r_t + \frac{t_s}{2}\right)\right]\cos\gamma \tag{8}$$

The coordinates of locations E-H on the member are as follows:

$$\begin{aligned}
E_x &= -g - l_4\cos\alpha + t_m \sin\alpha - \frac{d_{mh}}{2}\cos\alpha; & E_y &= -l_4 \sin\alpha + t_m \sin\alpha + \frac{d_{mh}}{2}\sin\alpha \\
F_x &= -g - l_4\cos\alpha + t_m \sin\alpha + \frac{d_{mh}}{2}\cos\alpha; & F_y &= -l_4 \sin\alpha + t_m \sin\alpha - \frac{d_{mh}}{2}\sin\alpha \\
G_x &= -g - l_4\cos\alpha - \frac{d_{mh}}{2}\cos\alpha; & G_y &= -l_4 \sin\alpha + \frac{d_{mh}}{2}\sin\alpha \\
H_x &= -g - l_4\cos\alpha + \frac{d_{mh}}{2}\cos\alpha; & H_y &= -l_4 \sin\alpha - \frac{d_{mh}}{2}\sin\alpha
\end{aligned} \tag{9}$$

The coordinates of locations I-L on the bottom plate are as follows:

$$\begin{aligned}
I_x &= l_6 \cos\beta + \frac{t_s}{2}\sin\beta - \frac{d_{ph}}{2}\cos\beta; \quad I_y = -\Big(l_6 - \frac{t_s}{2}\tan\beta\Big)\sin\beta + t_s\cos\beta - v_3 + \frac{d_{ph}}{2}\sin\beta \\
J_x &= l_6 \cos\beta + \frac{t_s}{2}\sin\beta + \frac{d_{ph}}{2}\cos\beta; \quad J_y = -\Big(l_6 - \frac{t_s}{2}\tan\beta\Big)\sin\beta + t_s\cos\beta - v_3 - \frac{d_{ph}}{2}\sin\beta \\
K_x &= l_6 \cos\beta - \frac{t_s}{2}\sin\beta - \frac{d_{ph}}{2}\cos\beta; \quad K_y = -\Big(l_6 - \frac{t_s}{2}\tan\beta\Big)\sin\beta - v_3 + \frac{d_{ph}}{2}\sin\beta \\
L_x &= l_6 \cos\beta - \frac{t_s}{2}\sin\beta + \frac{d_{ph}}{2}\cos\beta; \quad L_y = -\Big(l_6 - \frac{t_s}{2}\tan\beta\Big)\sin\beta - v_3 - \frac{d_{ph}}{2}\sin\beta
\end{aligned} \tag{10}$$

where l_6 is the length from the centerline to bottom plate hole centerline along the axis of the plate:

$$l_6 = \Big(\frac{l_2}{2} - l_3\Big) + \Big(r_b + \frac{t_s}{2}\Big)(\tan\beta - \beta) \tag{11}$$

Length v_3 is measured from the origin to the extension of the plate as drawn. This is different for each contact type (Figure 2E) for the bottom plate (B):

$$\begin{aligned}
&\text{Type B1 if: } \alpha \le \beta\text{ , } g - t_m\sin\alpha \le (r_b + t_s)\sin\beta\text{, and } \lambda \ge \alpha \\
&\text{Type B2 if: } \alpha \le \beta \text{ and } g - t_m\sin\alpha > (r_b + t_s)\sin\beta \\
&\text{Type B3 if: } \alpha > \beta \\
&\text{Type B4 if: } \alpha \le \beta\text{ , } g - t_m\sin\alpha \le (r_b + t_s)\sin\beta\text{, and } \lambda < \alpha
\end{aligned} \tag{12}$$

where λ is the angle from the center of curvature of the bottom plate to the point of contact with the member:

$$\lambda = \sin^{-1}\left(\frac{g - t_m\sin\alpha}{r_b + t_s}\right) \tag{13}$$

Length v_3 can be found as:

$$v_3 = \begin{cases} -r_b\cos\beta - r_b\sin\beta\tan\beta + \frac{t_m}{\cos\alpha} + v_4 & \text{if B1} \\ t_m\cos\alpha + \frac{t_s}{\cos\beta} - (g - t_m\sin\alpha)\tan\beta & \text{if B2} \\ \frac{t_s}{\cos\beta} + v_5 + \frac{t_m}{\cos\alpha} - v_6 & \text{if B3} \\ -r_b\cos\beta - r_b\sin\beta\tan\beta + t_m\cos\alpha + v_7 + (r_b + t_s)\cos\alpha & \text{if B4} \end{cases} \quad (14)$$

where v_4 is the vertical distance from the center of curvature of the bottom plate to the member contact location for case B1. Length v_4 is defined as follows:

$$v_4 = \sqrt{(r_b + t_s)^2 - \Big(\frac{g - t_m\sin\alpha}{2}\Big)^2} \quad (15)$$

The vertical distance between the contact point and the bottom corner of the member (v_5) for contact case B3 is:

$$v_5 = \Big(\frac{\frac{l_2}{2} + (r_b + \frac{t_s}{2})(\tan\beta - \beta)}{2}\cos\beta + \frac{t_s}{2}\sin\beta - g + t_m\sin\alpha\Big)\tan\beta \quad (16)$$

The vertical dimension of the bottom plate (v_6) for contact case B3 is:

$$v_6 = \frac{\frac{l_2}{2} + (r_b + \frac{t_s}{2})(\tan\beta - \beta)}{2}\sin\beta \quad (17)$$

The vertical distance between the contact point and the bottom corner of the member (v_7) for contact case B4 is:

$$v_7 = \Big((r_b + t_s)\sin\beta - g + t_m\sin\alpha\Big)\tan\alpha \quad (18)$$

Description of Parametric Investigation

A parametric investigation was performed as follows:

Level 1 - Connection Angle and Gap Analysis for Manufacturing and Erection Tolerances

The first level varies the member angle (α) and gap (g) between the members in order to determine the range of member connection angles and the minimum and maximum gap that are feasible for a given configuration. It is advantageous for the connection to achieve the widest range of member connection angles and to span the widest range of gaps between members to accommodate erection tolerances on both the angular and lateral placement of members.

For every combination of parameters of α and g, the feasibility of the configuration was evaluated for (1) member angles (α) plus or minus 5^o of the pre-bent splice plate angles (γ = β) in 0.5^o increments and (2) gaps (g) between a lower-bound based on a selected minimum clearance (e) and an upper-bound based on plate lengths (l_1 = l_2).

From a representative Level 1 analysis (Figure 3A), it is shown that with higher member angles (α) the range of allowable gap (g) is reduced. As a measure of the erection versatility, the area between the two lines indicating the minimum and maximum gap is calculated and recorded as C_{vers} (shaded region in Figure 3A) to be used in upper level geometric analyses.

Level 2 - Member Thickness and Depth for Versatility of Member Dimensions

A second level analysis considers the sensitivity of C_{vers} to varying member thicknesses (t_m) and member depth (d_m). This relates to the versatility of a design, allowing for the widest range of member sizes for a given configuration.

A representative Level 2 analysis (Figure 3B) shows that with lower member flange thicknesses (t_m) there is greater versatility (C_{vers}) than with higher member flange thicknesses. The considered member depths (d_m) have little effect on versatility. The volume beneath the surface of this plot is calculated and recorded as D_{vers} as a measure of the design versatility of the specified configuration to be used in upper level analyses.

Level 3 - Plate Lengths and Initial Angles

The third level of analysis considers the metric D_{vers} for a variety of plate lengths (l_1 = l_2) and initial plate angles (γ = β), as connections with higher angles require longer plates.

A representative Level 3 analysis (Figure 3C) shows that, up to a point, an increase in versatility can be achieved by increasing plate length. This is because the longer plate lengths allow deeper members to be connected without causing interference of the bottom flanges. To a lesser degree, it is shown that increasing plate angles (γ = β) decreases versatility, as was expected because the increased angles minimize available space for bolts to pass through the plated connection.

Level 4 - Radii of curvature and Member Hole Types

The fourth level analysis considers the radii of curvature (r_t = r_b) and member hole types (d_{mh}). The radii of curvature considered were 63.5 mm (2.5 in.) and 102 mm (4 in.). The former corresponds to the $5t$ minimum bend radii allowed by bridge design Code (AASHTO, 2012). The member hole types considered include oversized holes, short slots, and long slots.

This analysis repeats the Level 3 studies 6 times to evaluate all considered combinations of radii and member hole types. Results for r_t = r_b = 102 mm (4 in.) are shown in Figure 3D. Results for the smaller bend radius are not included as it was found that the value for the radius of curvature does not play a significant role in versatility. This is because in most configurations, the member contacts the straight portion of the plate resulting in the radius of curvature having minimal impact on the geometric analysis. It is shown that a significant improvement in versatility can be achieved through the use of long slots in the member, but short slots are very similar to oversized holes.

Results

The geometric parameters of the connection investigated in the experimental program were chosen based on the results of these studies. From the results of the Level 1 study (Figure 3A), it was found that higher member angles result in more stringent gap ranges to achieve feasibility. In the Level 2 study (Figure 3B), it was found that thicker member flanges result in reduced versatility, but member depth had little impact on versatility. The Level 3 study (Figure 3C) indicates that longer plates allow for deeper members to be connected by preventing interference of the bottom flange. From the Level 4 study (Figure 3D), it was found that the considered radii of curvature had little impact on the geometric analysis, and that longer slots in the member can dramatically increase the connection's versatility.

Based on these studies the member hole type is taken as a long slot [d_{mh} = 47.6 mm (1.875 in.)] to ensure the widest variety of feasible geometry. A 102 mm (4 in.) radius of curvature (r_t = r_b) was chosen as the radius does not significantly affect the versatility of the connection and larger bend radii reduce the magnitude of residual strains from prefabrication. The plate lengths (l_1 = l_2) were chosen for specific plate angles (γ = β) to achieve high versatility (D_{vers}). For γ = β

= 0^o, $l_1 = l_2$ = 381 mm (15 in.); for $\gamma = \beta = 5^o$, $l_1 = l_2$ = 432 mm (17 in.); for $\gamma = \beta = 10^o$, $l_1 = l_2$ = 483 mm (19 in.); for $\gamma = \beta = 15^o$ plates, $l_1 = l_2$ = 533 mm (21 in.). Note that the standard threaded length of A325 bolts can induce limitations for connections with large differences between the plate angles ($\gamma = \beta$) and member angle (α), as they require a significant threaded length to fully tighten the connection. Figure 4 shows the idealized geometry from this study and the as-built implementation, verifying this geometric study and highlighting its robustness.

EXPERIMENTAL PROGRAM

A total of 13 connection scenarios were tested to investigate the effect of the (1) bolt tightening procedure, (2) amount and direction of field bending, and (3) plate angle on the surface strains of the plates induced during field installation (Table 2, Figure 4). Scenario 1 was tested three times to demonstrate repeatability. All other scenarios were tested once.

Each scenario used three ASTM A36 steel plates to connect the top flanges of two W10x88 beams (Figure 5). A single top plate [12.7 mm (0.500 in.) thick by 203 mm (8.00 in.) wide with lengths varying from 381 to 533 mm (15.0 to 21.0 in.)] connected the top surface of the top flanges, while two bottom plates [12.7 mm (0.500 in.) thick by 76.2 mm (3.00 in.) wide with lengths varying from 381 to 533 mm (15.0 to 21.0 in.)] connected the underside of the top flanges, with one bottom plate located on each side of the web of the beams. The plates were pre-bent via a press brake and the residual strains induced during prefabrication were reported in Gerbo et al. (2016b). Each connection used four ASTM A325 19.1 mm (0.750 in.) diameter bolts. The stress strain relationships of A36 plate and A325 bolt specimens, found according to ASTM standards A370 and F606 respectively (ASTM, 2015, 2014), are shown in Figure 6. Bolt testing was performed by Laboratory Testing Inc. (Laboratory Testing Inc., 2017). A325 bolts were selected as these are the most commonly used high-strength bolt (Salmon et al., 2009) and feature enhanced ductility and lower susceptibility to stress corrosion and hydrogen stress cracking when galvanized in comparison to higher strength bolts (*e.g.*, A490) (Kulak et al., 2001). Further, the Federal Highway Administration (FHWA) recommends the use of A325 bolts over A490 (FHWA, 2015a) and bridge design Code prohibits the use of galvanized A490 bolts (FHWA, 2015b; AASHTO, 2014).

Each W10x88 beam was supported by a W10x88 stub column connected to a W12x106 grade beam that was anchored to the laboratory floor (Figure 5). Different stub columns were used to vary the angle of the beams. Bolts were tightened manually via a torque wrench, with the assistance of a torque multiplier (Figure 5B). One W6x12 cantilevered column was located at each end of the test setup and bolted to the laboratory floor. These columns provided a reaction point for the tools used to tighten the bolts and support the instrumentation system (Figure 5B and 5C). Figure 4 shows the idealized geometry as well as the experimental setup for each tested scenario. In all scenarios the bolts fit into the assembly as anticipated, verifying the accuracy of the geometric study.

The full-field surface strains in the plates were measured using DIC, a non-contact optical technique. The 3D DIC system (provided by Trilion Quality Systems) consisted of two cameras [2448 x 2050 pixels with 12.0 mm (0.472 in.) manual focus lenses] and utilized ARAMIS DIC software to measure surface strains within the field-of-view (FOV). Multiple camera positions and mirrors were used to capture the behavior of the top surface of the top plate and bottom surfaces of both bottom plates (Figure 5C). The FOV for each position was approximately 610 by 510 mm (24.0 by 20.1 in.). Stereo pairs of photographic images were captured and divided into regions called facets that are 13 by 13 pixels. Using photogrammetric triangulation and pattern recognition, these facets were tracked through a series of images to produce 3D full-field surface strains. Overall, the system is capable of measuring strains up to 0.0001 mm/mm (0.0001 in./in.) (TRILION, 2016).

There were several challenges in the application of DIC to this research. In general, DIC requires a clear view of any measured surface from both cameras. However, in this research the bolt assemblies block a portion of the steel plates from view of the cameras, causing some minor data loss. Camera positions were optimized to reduce data loss as much as possible. In addition, the DIC pattern is typically achieved by painting the specimen with a white background and black dots. In this research, the plates were bent using a press brake, resulting in surface abrasion that traditional DIC paint could not withstand. Instead, the surface was first coated with CerMark

LMM-6000 Metal Laser Marking Spray (Ferro, 2016) and then etched with a durable random pattern using a laser cutter (Universal Laser Cutter, VLS 6.60, 50W laser) as was done in Gerbo et al. (2016b). This surface preparation resulted in significant specular reflection. This resulted in challenges with the lighting during testing, as both cameras must not only be able to clearly see the plate, but also must have similar lighting/reflection to enable the algorithm to correlate locations between the two images. The authors recommend using careful lighting when specularly reflective surfaces are tested.

BEHAVIOR DURING FIELD BENDING

Effect of Bolt Tightening Procedure

This section focuses on the impact of the bolt tightening procedure on the surface strains induced in the plates during field installation. As shown in Table 2, five different bolt-tightening procedures were investigated (Scenarios 1-5) when bending plates from $\gamma = \beta = 10°$ to $\alpha = 17.5°$. The difference between plate angles ($\gamma = \beta$) and member angles (α) is defined as δ, and considered positive when the member angle is greater than the plate angles (*e.g.*, for Scenarios 1-5, $\delta = +7.5°$). For each scenario, the connection was considered fully tightened when the turn-of-nut criteria (AASHTO, 2010) was satisfied for each individual bolt.

Figure 7 shows a plan view of the top and bottom plates and indicates four longitudinal lines for which data will be presented: line A is the centerline of bottom plate 1 (BP1), line B intersects the top row of bolts for the top plate (TP), line C intersects the bottom row of bolts for the top plate, and line D is the centerline of bottom plate 2 (BP2).

Figure 8 displays the measured circumferential surface strains (ϵ_x) as a function of the location along lines A-D for Scenarios 1, 2, 4, and 5. The magnitudes of strains are very similar in both the top and bottom plates [around 0.03 mm/mm (0.03 in./in.)] for all scenarios. As expected, the peak strains in the top plate occur near the point of contact with the beams (shown as dashed vertical lines) and have relatively narrow widths [approximately 30 to 40 mm (1.2 to 1.6 in)]. The peak strains in the bottom plates occur at the edge of the pre-bent region (indicated by the gray-shaded region). These peaks are on the edges of the pre-bent region which has been work hardened and therefore has a higher yield strength as opposed to the straight portions of the plate. There are also strains measured throughout the pre-bent region, as the bottom plates behave similar to a beam under four-point bending.

The measured strains from the three tests of Scenario 1 (identified as Scenarios 1a, 1b, and 1c) were very similar, demonstrating that the connection assembly and bolt tightening procedure are repeatable. With repeatability demonstrated, only one test of all other scenarios was performed.

The left column of Figure 9 shows the progression of strain during the bolt tightening process of Scenario 1, while the right column shows the final strain induced by the bolt tightening procedures of Scenarios 1, 4, and 5 (criss-cross, clockwise, and counter-clockwise, respectively). Figure 9 (left) shows the full-field surface strains within the DIC FOV in the top and bottom plates for Scenario 1, with the measured results shown after six turns of each bolt, at the point of contact between the plates and the beams, and after the final turn of the bolts (when the turn-of-nut criteria was satisfied). As expected, the strain in the top plate increases in magnitude as the bolts are tightened. However, the net section of the bottom plate (near the bolt holes) experiences a peak strain after six turns, then decreases in magnitude as the bolts are further tightened. During bolt tightening, the bottom plate starts to bend and moves towards the member with minimal initial deformations at the center of the bottom plate. Once the bottom plate comes into contact with the member, the deformations at the center of the plate become more dominant and reach peak strain after the final bolt turn. The hysteresis in the net section of the bottom plates during installation must be accounted for during design, as it enhances the potential for reduced ductility and fatigue resistance of the steel in the cold-worked region.

Increment of Tightening

Scenarios 1, 2, and 3 all used the criss-cross tightening pattern, but with varying increments (or number) of turns at a time. While Scenario 1 and 2 resulted in very similar strain patterns, it was observed in Scenario 2 that tightening in larger increments (three turns per tightening step) resulted in noticeable gouging of the bolts. Scenario 3 (in which bolts were fully tightened individually) is not plotted on Figure 8 because bolt 3 fractured during the tightening process. Therefore, it is recommended only one full turn of an individual bolt at a time be implemented.

Pattern of Tightening

Scenarios 4 and 5 use clockwise and counter-clockwise tightening patterns, respectively, as compared to Scenario 1, which uses the criss-cross pattern. The measured strains in Scenarios 1, 4, and 5 are very similar, as shown in Figure 8 and in Figure 9. However, there is some asymmetry in the peak strains on the bottom plate which changes location based on the tightening pattern. This asymmetry is more pronounced in the bottom plate as the bottom plates are restrained by just two bolts and are therefore more susceptible to differences in the order in which bolts are tightened, compared to the top plate. This is more pronounced in Scenario 4 and 5 which feature circular tightening patterns as opposed to Scenario 1 which uses the criss-cross pattern. Further, some strain bands occur near the net section of the top plate for Scenarios 4 and 5. This is not desirable as it may reduce fatigue resistance of the connection. As a result, the criss-cross pattern is recommended over circular patterns.

In general the peak strains are not significantly affected by tightening procedure, therefore the recommended tightening procedure is one turn per increment, with a criss-cross tightening pattern.

Effect of Amount and Direction of Field Bending

This section investigates the impact of the amount (*i.e.*, number of degrees δ) and direction (*i.e.*, increasing or decreasing the angle of the pre-bent plate) on the surface strains induced in the connection. As shown in Table 2, four different member angles were investigated (Scenarios 1 and 6-8), with Scenario 1 serving as the baseline for comparison of the measured behaviors. Each scenario used the same bolt tightening procedure as Scenario 1 (*i.e.*, one full turn of an individual bolt at a time, using a repeated crisscross pattern to tighten the entire four bolt connection).

Figure 10 (left) shows the measured circumferential surface strains during field bending as a function of the location along lines A-D and Figure 11 shows the full-field strains. As expected, compressive strains developed in the top plate while tensile strains developed in the bottom plate for Scenarios 1 and 6 (where $\delta > 0$). Similarly, for Scenarios 7 and 8 (where $\delta < 0$), compressive strains developed in the bottom plate while tensile strains developed in the top plate. Also as expected, the highest absolute peak strains occurred when the magnitude of the field bend (δ) was largest. The overall peak strain [approximately 0.035 mm/mm (0.035 in./in.)] is observed in Scenario 1 in the top plate near the point of contact with the beams (shown as dashed vertical lines). In Scenario 8, the peak strain [approximately 0.02 mm/mm (0.02 in./in.)] occurred in the net section of the top plate. This is an important feature as the cold working here would reduce the ductility of the plate at the net section (bolt holes) enhancing the potential for reduced fatigue resistance of the steel in the cold-worked region. This was not observed in the plots in Figure 10 due to data loss along lines B and C (where the section cut goes through the holes in the plate as shown in Figure 7). The bolt assembly also blocks a portion of the DIC view of the plate due to the washers being larger diameter [37.0 mm (1.46 in.)] than the holes in the plates [23.8 mm (0.938 in.)].

The peak strains in the bottom plates occur at the edge of the pre-bent region for Scenario 1, but occur in the center pre-bent region and near the line of contact with the beams for Scenario 8. Scenario 8 creates a region of constant moment in between the point of contact with the member, and thus the plateau in the center is expected. In Scenario 8, there are no double peaks in strain around the pre-bent region, as observed in Scenario 1. This is due to Scenario 8 inducing bending in the direction opposite the direction of prefabrication. Here, the Bauschinger effect is lowering the yield stress in the pre-bent region. While the magnitude of this peak strain was smaller, the distribution of plastic strains was much wider (covering the entire pre-bent region of the bottom plate). Figure 11 shows that some minor strain banding occurs across the top plates outside the pre-bent region, this is believed to be due to inhomogeneity in the grain structure of the steel. Scenarios 6 and 7 (featuring δ = +2.5° and -2.5° field bends, respectively) had very small measured peak strains [around 0.005 mm/mm (0.005 in./in.)], indicating that small field bends do not generate significant surface strains. To minimize the induced strains, connections with $\delta = \pm\ 2.5°$ or lower are recommended.

The right column of Figure 10 shows the cumulative strains [*i.e.*, strains from field installation plus residual strains from pre-fabrication]. These cumulative strains reach peak magnitudes of approximately 0.07 mm/mm (0.07 in./in.) in the bottom plates of Scenario 1. The bottom plates of Scenario 1 experience the highest cumulative strain because the induced strains from field bending and prefabrication occur in the same region, and the strains are additive because $\delta > 0$. In the top plates of Scenario 1, the strain induced during field bending is in a different location than the strain from prefabrication, hence the three distinct peaks along lines B and C. Conversely, Scenario 8 experiences a decrease in magnitude of cumulative strain because $\delta < 0$.

Understanding the cumulative final strain and hysteresis induced are important design factors. Previous studies have found that plastic strains up to 0.10 mm/mm (0.10 in./in.) resulted in minimal effect on ductility and fracture toughness (Keating and Christian, 2012). The measured strains in this study are below this upper limit. Fatigue behavior of steel is not only dependent on applied cyclic load, but also on loading history (Erber et al., 1992). The plastic strains induced during prefabrication and field installation will have an effect on components subjected to fatigue loading; therefore, strain history must be taken into consideration during the design process. In many of the tested scenarios, the locations of induced plastic strain are not coincident with critical areas of the splice plates (*i.e.*, the net section across bolt holes), and are not likely to significantly affect the overall design of the connection. The cumulative induced plastic strains will result in reduced fracture toughness and ductility, including also the effect of strain aging (FHWA, 2015b). Strain hysteresis produces additional micro-defects that can reduce fatigue life and must be considered in design (FHWA 2015b, Erber et al. 1992). The quantitative impact on fatigue performance is an area for future research.

Effect of Varying Plate Angles

This section investigates the effect of different plate angles. All scenarios discussed here use the same bolt tightening procedure as Scenario 1. As shown in Table 2, four different plate angles were investigated: Scenario 1, 9-13. All feature small bend angles (δ = $\pm 2.5°$) and therefore have low strains [with peaks on the order of 0.01 mm/mm (0.01 in./in.)].

As shown in Figure 12, the peak magnitude of strain in Scenario 9 occurs in the top plate near the point of contact with the beam on the right side. This asymmetry can be attributed to slight differences in the height of members in the reaction frame. This scenario is particularly susceptible to slight imperfections in the reaction frame as the plates are initially flat.

In Scenario 10, peak strains occur near the center (within the pre-bent region) of the bottom plates. This is consistent with the behavior observed in Scenario 8 which also has a $\delta < 0$. Scenario 11, which has a $\delta > 0$, exhibits small strain concentrations in the top plate near the line of contact with the member, as expected and consistent with Scenario 1.

Figure 13 displays the measured surface strains for Scenarios 12 and 13. In Scenario 12, strains are mostly negligible. Scenario 13 experiences higher magnitudes of strain approaching 0.01 mm/mm (0.01 in./in.), with peaks in the bottom plates at the center, and in the top plates at the lines of contact with the member. This pattern is consistent with that observed in Scenario 1.

Overall, this section demonstrates that varying the level of initial pre-bend has little impact on the strains induced during field installation. Rather the amount and direction of bend, as investigated in the prior section, are more important.

RECOMMENDATIONS AND CONCLUSIONS

This paper investigated an adjustable bolted steel plate connection to join a range of angled steel members. The connection features pre-bent plates that are further bent during field installation via bolt tightening. This research focused on the field installation process following prior work by the authors on prefabrication (Gerbo et al., 2016b). An extensive, four-level geometric study was performed to select ideal connection parameters, resulting in the following conclusions:

- Larger member angles reduce the allowable gap between members. In this study member angles (α) up to 17.5° were found to result in feasible geometries.
- The versatility of a connection (*i.e.*, range of feasible parameters within a connection) can be increased by using (1) members with thinner flanges [*e.g.*, t_m less than 25.4 mm (1.0 in.)], (2) longer plates [*e.g.*, l_1 = l_2 greater than 432 mm (17 in.)], or (3) longer slots [*e.g.*, d_{mh} = 47.6 mm (1.875 in.)].
- Increasing the plate angle will probably decrease the versatility of a connection. This re-

relationship has minimal effect at low plate angles (*i.e.*, $\gamma = \beta = 0°$ and 5°), with a more significant effect at higher angles (*i.e.*, $\gamma = \beta = 10°$ and 15°).

- The considered radii [$r_t = r_b$ = 63.5 mm and 102 mm (2.50 in. and 4.00 in. respectively)] of curvature do not play a significant role in the versatility of a connection.

Using selected connection parameters based on these geometric analyses, a total of 13 different full-scale connection scenarios were tested to understand the impact of the (1) bolt tightening procedure, (2) amount and direction of field bending, and (3) plate angle on the surface strains induced during field installation. Strains were measured using DIC to capture full-field behavior. Based on these experimental tests, the following conclusions and recommendations are made:

- The preferred bolt tightening procedure features one full turn per tightening increment in a repeated criss-cross pattern to tighten the four-bolt connection. Tightening in larger increments resulted in noticeable gouging or fracture of the bolts. Tightening in circular patterns resulted in more asymmetry of strain patterns.
- The authors recommend limiting connections to $\delta = \pm\, 2.5°$ as they were found to minimize induced strain, representing a reasonable limit to fabrication tolerances for bent plates. Residual strains from prefabrication must also be considered.
- For plates where the field bend increased the angle of the plates, the peak strains typically occurred in the top plate near the point of contact with the member. For plates where the field bend decreased the angle of the plates, the peak strains typically occurred within the pre-bent region of the bottom plate.
- High strains were observed in the net section area of the bottom plate during the tightening process for plates where the field bend increased the angle of the plates. For plates where the field bend decreased the angle of the plates, high strains occurred in the net section area of the top plate. These regions require additional attention during design as there is enhanced potential for reduced ductility and fatigue resistance of the steel in the cold-worked region. For connections subject to high cycle fatigue, this may limit acceptable

field bending angles (δ).

- The peak induced strain during field bending depends primarily on δ. Only varying the plate angle had negligible effect induced on strains.

These measured results using DIC have provided an unprecedented understanding of this field installation procedure. Additionally the results are relevant to cold bent double shear connections in general and also useful for assessing their behavior and setting bend tolerances for fabrication. Future work will focus on understanding the behavior of these connections under design and service loads, including fatigue performance and both numerical and experimental research.

ACKNOWLEDGMENTS

This material is based upon work supported by the National Science Foundation under Grant No. CMMI-1351272. The support of Program Managers Drs. Kishor Mehta and Y. Grace Hsuan is gratefully acknowledged. The authors are grateful to the University of Notre Dame Equipment Restoration and Renewal Program which funded the purchase of the DIC system. The authors are also grateful to Builders Iron Works, Inc. for fabricating and press braking the samples at a reduced cost, as well as Alro Steel for providing the steel at a reduced cost.

REFERENCES

AASHTO (2010). *AASHTO LRFD Bridge Construction Specifications*. American Association of State Highway and Transportation Officials (AASHTO), 3rd Edition, with 2010, 2011, 2012, 2014, 2015 and 2016 Interim Revisions, Washington, D.C.

AASHTO (2012). *AASHTO LRFD Bridge Construction Specifications*. American Association of State Highway and Transportation Officials (AASHTO), 2012 Interim Revisions to 3rd Edition, Washington, D.C.

AASHTO (2014). *AASHTO LRFD Bridge Design Specifications, Customary U.S. Units*. American Association of State Highway and Transportation Officials (AASHTO), 7th Edition, with 2015 and 2016 Interim Revisions, Washington, D.C.

ASTM (2014). "ASTM F606/606M-14a: Standard test methods for determining the mechanical properties of externally and internally threaded fasteners, washers, direct tension indicators, and rivets." ASTM International. West Conshohocken, PA.

ASTM (2015). "ASTM A370-14: Standard test methods and definitions for mechanical testing of steel products." ASTM International. West Conshohocken, PA.

Chung, K. F. and Lau, L. (1999). "Experimental investigation on bolted moment connections among cold formed steel members." *Engineering Structures*, 21(10), 898–911.

Cota, K. and Zoli, T. P. (2012). "Bridge design: Truss with a twist." *Roads & Bridges*, 50(12), 22–24,26–27.

Davies, J. M. (2000). "Recent research advances in cold-formed steel structures." *Journal of Constructional Steel Research*, 55(1-3), 267–288.

Erber, T., Guralnick, S. A., and Michels, S. C. (1992). "Hysteresis and fatigue." *Annals of Physics*, 224(2), 157–192.

Ferro (2016). “CerMark laser marking materials. http : //www.ferro.com/Our + Products/ColorsGlass/FunctionalIndustrial/CerMark/ (January 26, 2016).

FHWA (2015a). “High Strength Bolts. https : //www.fhwa.dot.gov/bridge/boltsqa.cfm (June 13, 2017).

FHWA (2015b). *Steel Bridge Design Handbook: Bridge Steels and their Mechanical Properties*. U.S. Department of Transportation, Federal Highway Administration (FHWA), Washington, D.C.

FHWA (2015c). *Steel Bridge Design Handbook: Steel Bridge Fabrication*. U.S. Department of Transportation, Federal Highway Administration (FHWA), Washington, D.C.

Gerbo, E. J., Casias, C. M., Thrall, A. P., and Zoli, T. P. (2016a). “New bridge forms composed of modular bridge panels.” *American Society of Civil Engineers Journal of Bridge Engineering*, 21(4), 04015084.

Gerbo, E. J., Thrall, A. P., Smith, B. J., and Zoli, T. P. (2016b). “Full-field measurement of residual strains in cold bent steel plates.” *Journal of Constructional Steel Research*, 127, 187–203.

Gergess, A. N. and Sen, R. (2005a). “Cold curving symmetric unstiffened I-girders.” *Journal of Constructional Steel Research*, 61(4), 473–492.

Gergess, A. N. and Sen, R. (2005b). “Fabrication of unsymmetrical curved plate girders by cold bending.” *Journal of Constructional Steel Research*, 61(10), 1353–1372.

Gergess, A. N. and Sen, R. (2008). “Cold curving steel bridge girders.” *Journal of the Transportation Research Board*, 2081, 165–175.

Gergess, A. N. and Sen, R. (2009). “Cold bending HPS 485W steel bridge girders.” *Journal of Constructional Steel Research*, 65(8-9), 1549–1557.

Hancock, G. J. (2003). “Cold-formed steel structures.” *Journal of Constructional Steel Research*, 59(4), 473–487.

HNTB Corporation, Genesis Structures, Inc., Structural Engineering Associates, Iowa State University (2014). *Strategic Highway Report S2-R04-RR-1 Innovative Bridge Designs for Rapid Renewal*. Transportation Research Board, Washington, D.C.

Keating, P. B. and Christian, L. C. (2012). "Effects of bending and heat on the ductility and fracture toughness of flange plate. Technical Report No. FHWA/TX-10/0-4624-2.

Kulak, G. L., Fisher, J. W., and Struik, J. H. A. (2001). *Guide to Design Criteria for Bolted and Riveted Joints*. American Institute of Steel Construction, 2nd Edition, Chicago, I.L.

Laboratory Testing Inc. (2017). "Tensile Testing. https : //www.labtesting.com/services/materials − testing/mechanical − testing/tensile − testing/ (June 13, 2017).

Pedreschi, R. F., Sinha, B. P., and Davies, R. (1997). "Advanced connection techniques for cold-formed steel structures." *Journal of Structural Engineering*, 123(2), 138–144.

Salmon, C. G., Johnson, J. E., and Malhas, F. A. (2009). *Steel Structures: Design and Behavior*. Pearson Education Inc., 5th Edition, Upper Saddle River, N.J.

TRILION (2016). "The Theory of Digital Image Correlation. http : //trilion.com/digital − image − correlation − theory/ (August 16, 2016).

TXDOT (2015). "Preferred practices for steel bridge design, fabrication, and erection. Texas Deparment of Transportation (TXDOT), Texas Steel Quality Council.

Yu, W. W. and LaBoube, R. A. (1997). "University of missouri-rolla research on cold-formed steel structures." *Thin-Walled Structures*, 28(3/4), 213–223.

Yu, W.-W., Wolford, D. S., and Johnson, A. L. (1996). "Golden anniversary of the AISI specifcation." *Proceedings of the Thirteenth International Specialty Conference on Cold-Formed Steel Structures*, 1–25.

List of Tables

Symbol	Definition	Values Investigated
Plate Geometry		
γ	Top plate angle	0°, 5°, 10°, and 15°
β	Bottom plate angle	β=γ
l_1	Top plate length	305 mm - 559 mm (25.4 mm increments) [12 in. - 22 in. (1 in. increments)]
l_2	Bottom plate length	l_2=l_1
r_t	Top plate radius	63.5 mm, 102 mm [2.5 in., 4 in.]
r_b	Bottom plate radius	r_b=r_t
t_s	Plate thickness	12.7 mm (0.5 in.)
d_{ph}	Plate hole length	Oversized holes: 23.8 mm (0.9375 in.)
l_3	Plate hole end distance	76.2 mm (3 in.)
Member Geometry		
t_m	Member thickness	12.7 mm - 38.1 mm (3.18 mm increments) [0.5 in. - 1.5 in. (0.125 in. increments)]
d_m	Member depth	203 mm, 254 mm, and 305 mm (8 in., 10 in., and 12 in.)
d_{mh}	Member hole length	Oversized holes: 23.8 mm (0.9375 in.) Short slots: 25.4 mm (1 in.) Long slots: 47.6 mm (1.875 in.)
l_4	Member hole end distance	76.2 mm (3 in.)
Connection Configuration		
α	Member angle	α = $\gamma \pm 5°$ (0.5° increments)
g	Gap between members	($g \geq d_m \sin\alpha + e$) - max (0.794 mm increments, e=3.18 mm) (0.03125 in. increments, e=0.125 in.)
d_b	Bolt diameter	19.1 mm (0.75 in.)

TABLE 1. Geometric parameters for connection, including values for parametric investigation. See Figure 2A and 2B.

	$\gamma = \beta$ (deg.)	α (deg.)	δ (deg.)	l_1=l_2 (mm)	Tightening Procedure increment (pattern*)
1	10	17.5	7.5	483	1 turn/bolt (x)
2	10	17.5	7.5	483	3 turns/bolt (x)
3	10	17.5	7.5	483	Fully tighten bolt (x)
4	10	17.5	7.5	483	1 turn/bolt (cw)
5	10	17.5	7.5	483	1 turn/bolt (ccw)
6	10	12.5	2.5	483	1 turn/bolt (x)
7	10	7.5	-2.5	483	1 turn/bolt (x)
8	10	2.5	-7.5	483	1 turn/bolt (x)
9	0	2.5	2.5	381	1 turn/bolt (x)
10	5	2.5	-2.5	432	1 turn/bolt (x)
11	5	7.5	2.5	432	1 turn/bolt (x)
12	15	12.5	-2.5	533	1 turn/bolt (x)
13	15	17.5	2.5	533	1 turn/bolt (x)

TABLE 2. Summary of connection scenario parameters. * Abbreviations for bolt tightening procedure, with indications for bolt number (Figure 7): (x) = criss-cross (1-2-3-4), (cw) = clockwise (1-4-2-3), (ccw) = counter-clockwise (4-1-3-2).

List of Figures

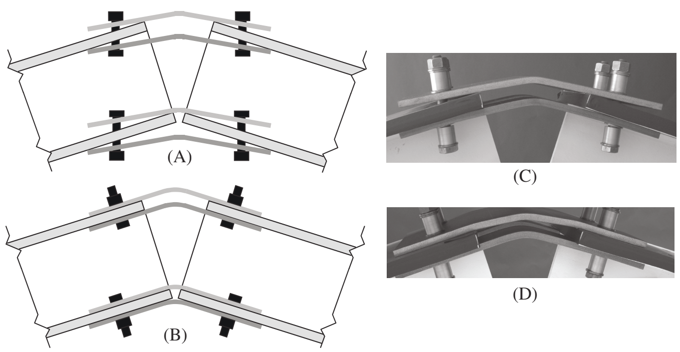

FIG. 1. Field bending: (A) rendering of initial un-tightened connection; (B) rendering of final tightened connection; (C) photograph of initial un-tightened connection (Scenario 1); (D) photograph of final tightened connection (Scenario 1).

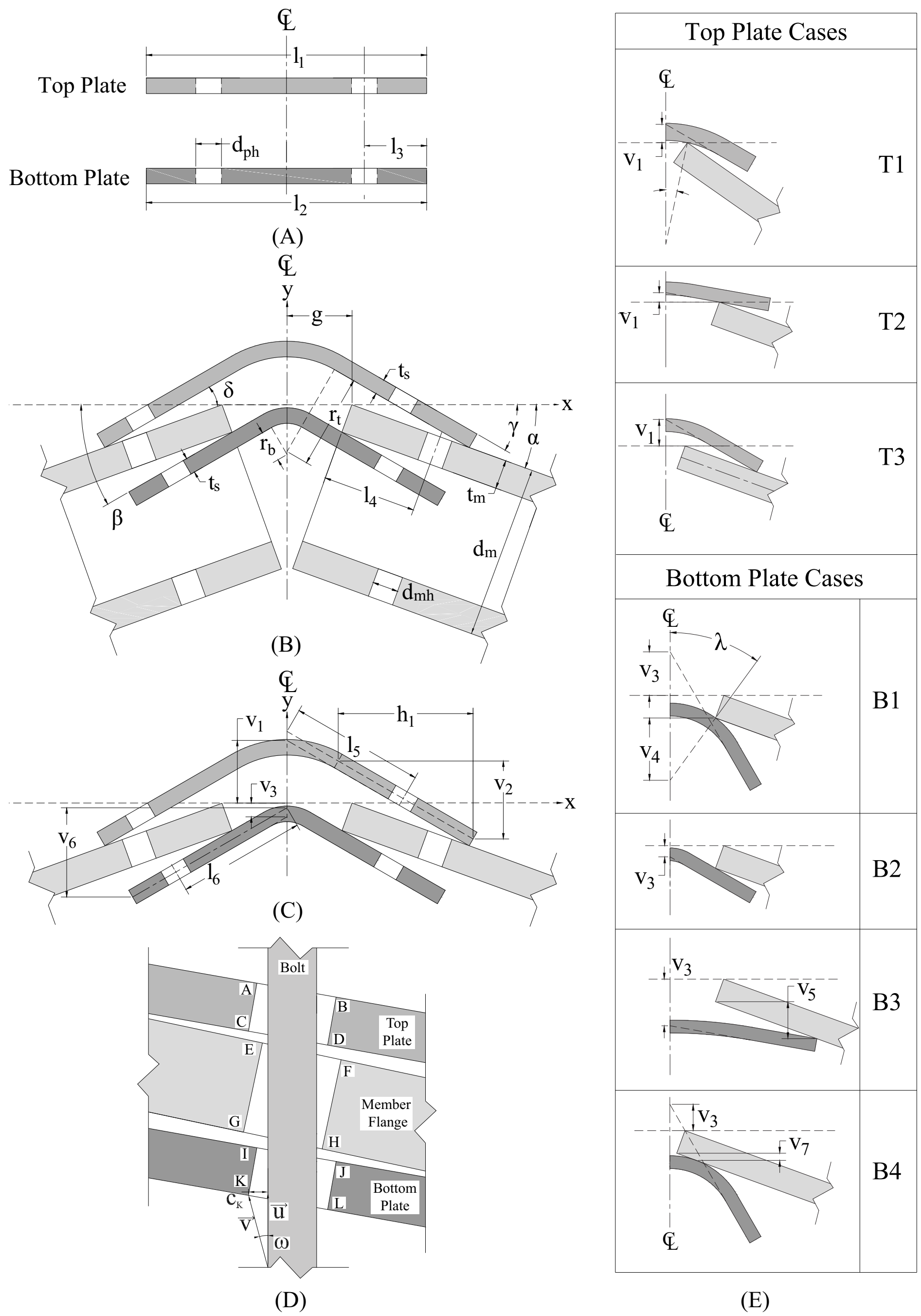

FIG. 2. Geometric definition of the connection, including definition of parameters and related variables for (A) flat plate and (B,C) bent plates (configuration exaggerated to show dimensions), (D) definition of locations A-L, including example vectors $\vec{u}$, $\vec{v}$ and angle ω are shown for c_K, and (E) contact case definitions [only one plate (dark gray) and the member (light gray) are shown for simplicity].

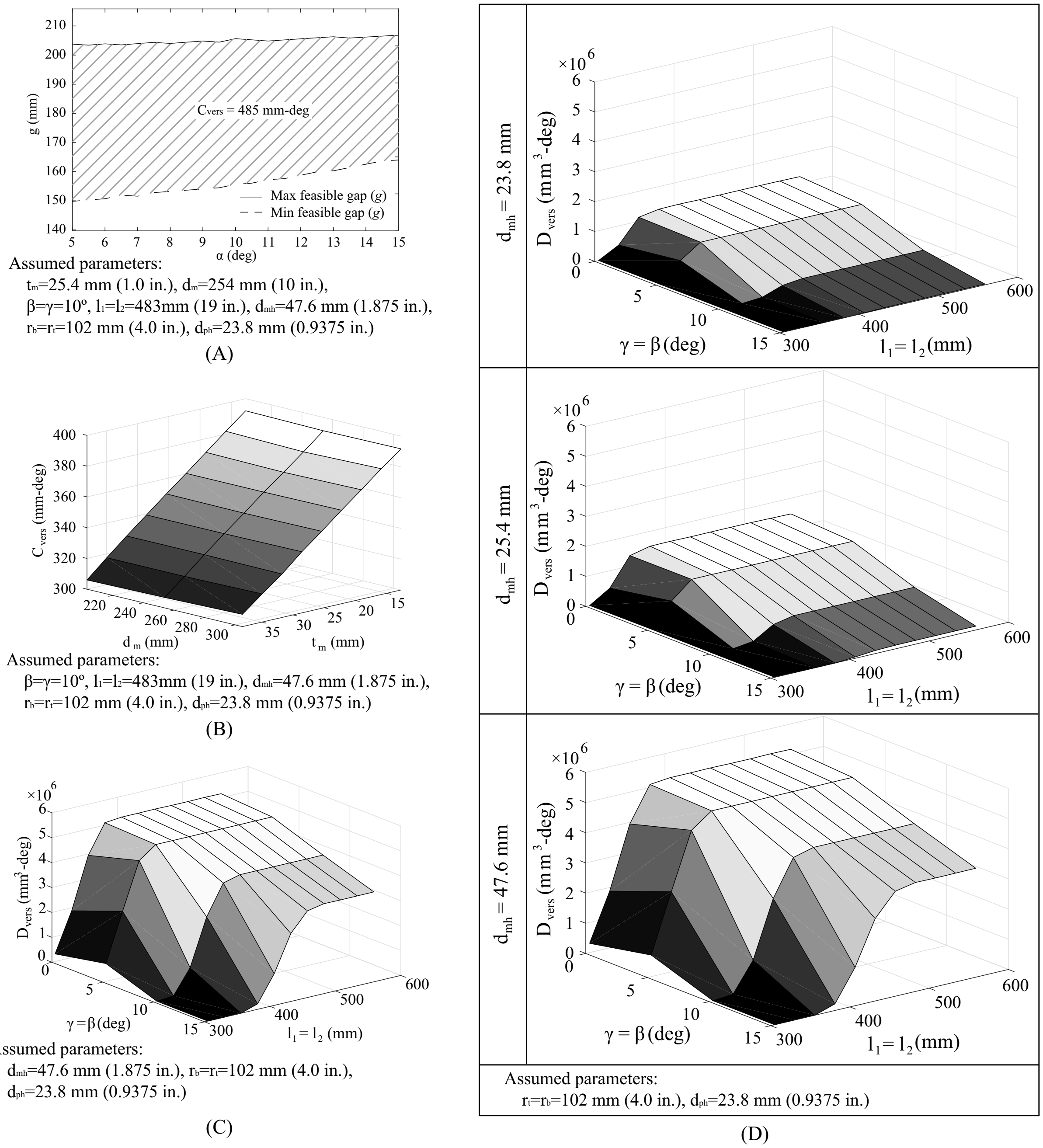

FIG. 3. Geometric analysis results, including (A) representative Level 1 analysis considering connection angle (α) and gap (g), (B) representative Level 2 analysis considering member depth (d_m) and member thickness (t_m), (C) representative Level 3 analysis considering plate length (l_1 = l_2) and initial plate angle (β = γ), and (D) representative Level 4 analysis considering member hole type (d_{mh}). Note: the color scale is proportional to the versatility metric on the vertical axis for (B), (C), and (D).

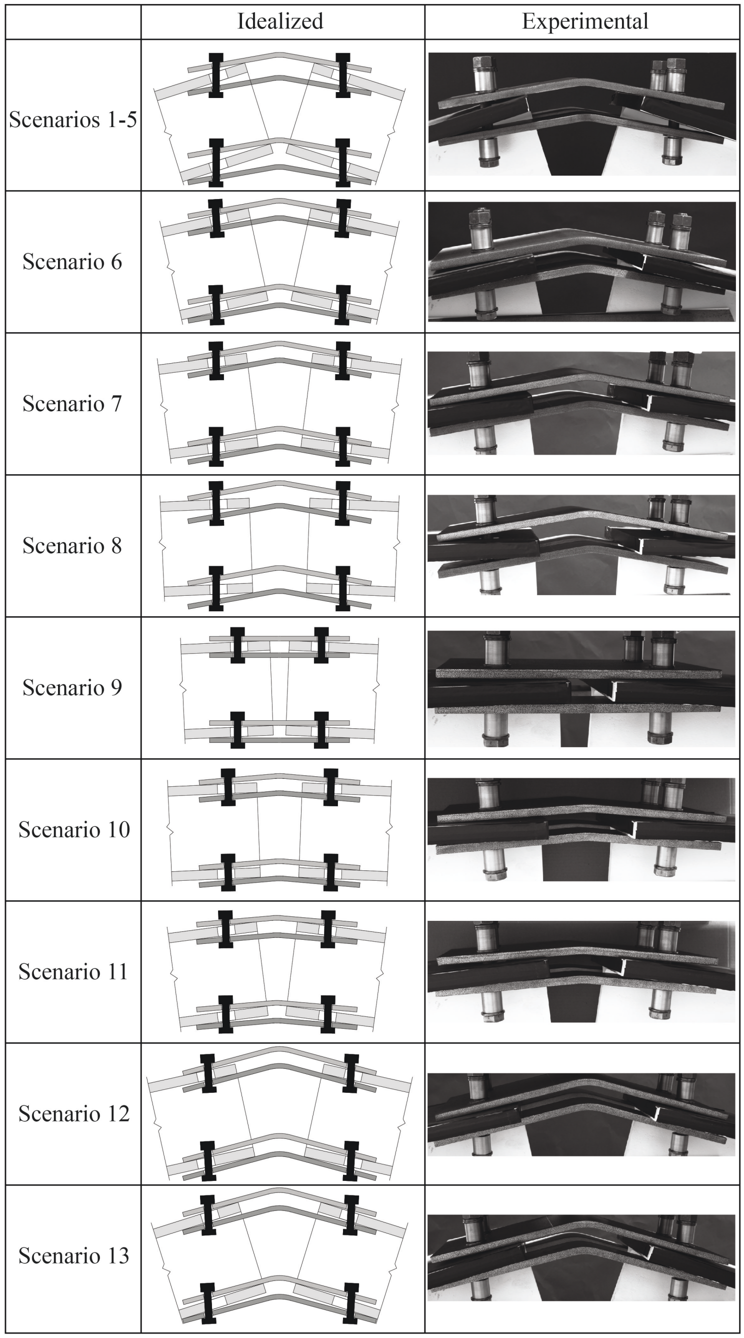

FIG. 4. Rendering of idealized geometry (left) and photograph of the experimental setup (right) for each tested Scenario.

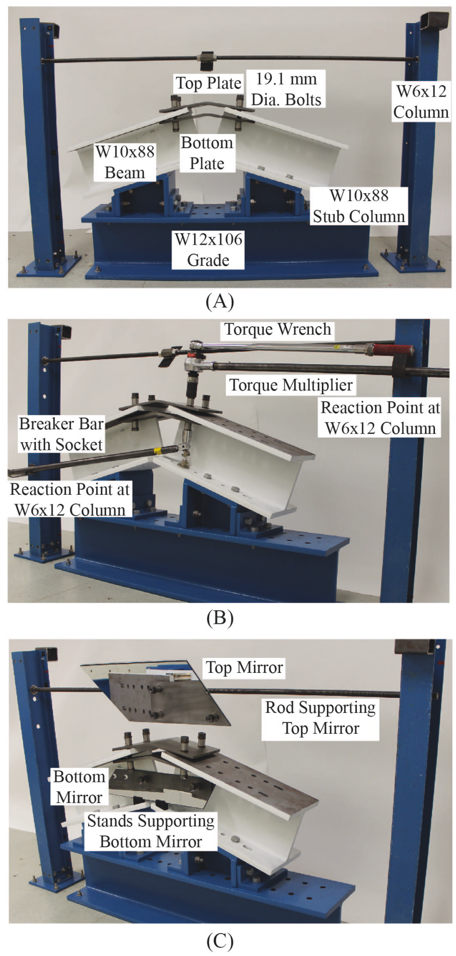

FIG. 5. Experimental test setup shown for Scenario 1, including (A) elevation view, (B) bolt tightening tools, and (C) instrumentation support system.

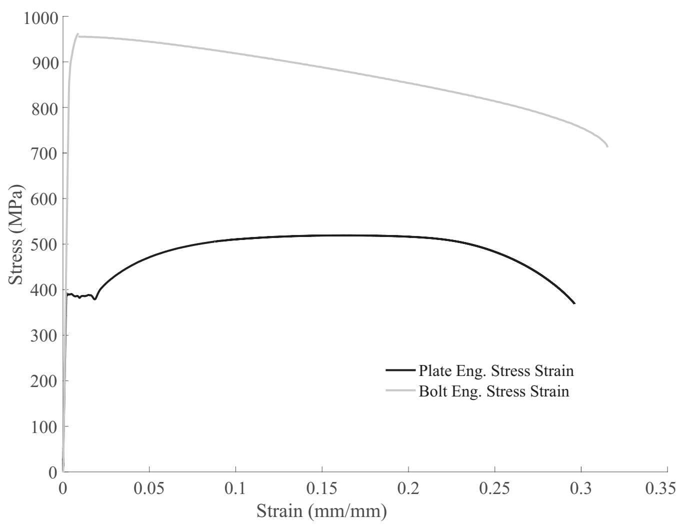

FIG. 6. Measured engineering stress-strain relationships for a representative plate and bolt. Plate data reprinted from Journal of Constructional Steel Research, 127, EJ Gerbo, AP Thrall, BJ Smith, and TP Zoli, Full-field Measurement of Residual Strains in Cold Bent Steel Plates, 187-203, 2016, with permission from Elsevier.

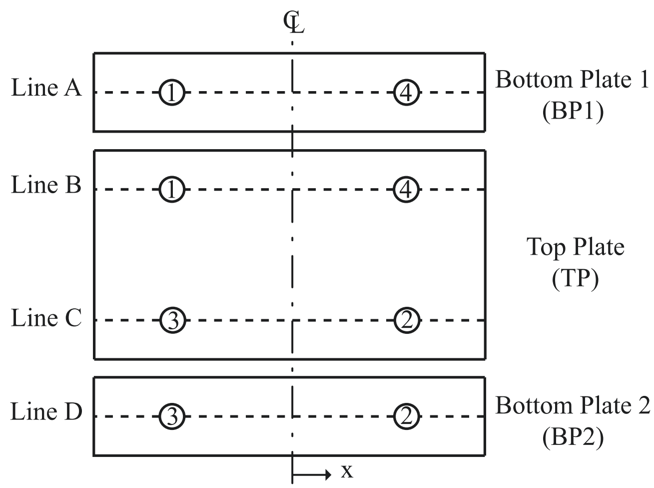

FIG. 7. Longitudinal lines for data identification. Numbers indicate bolt identification.

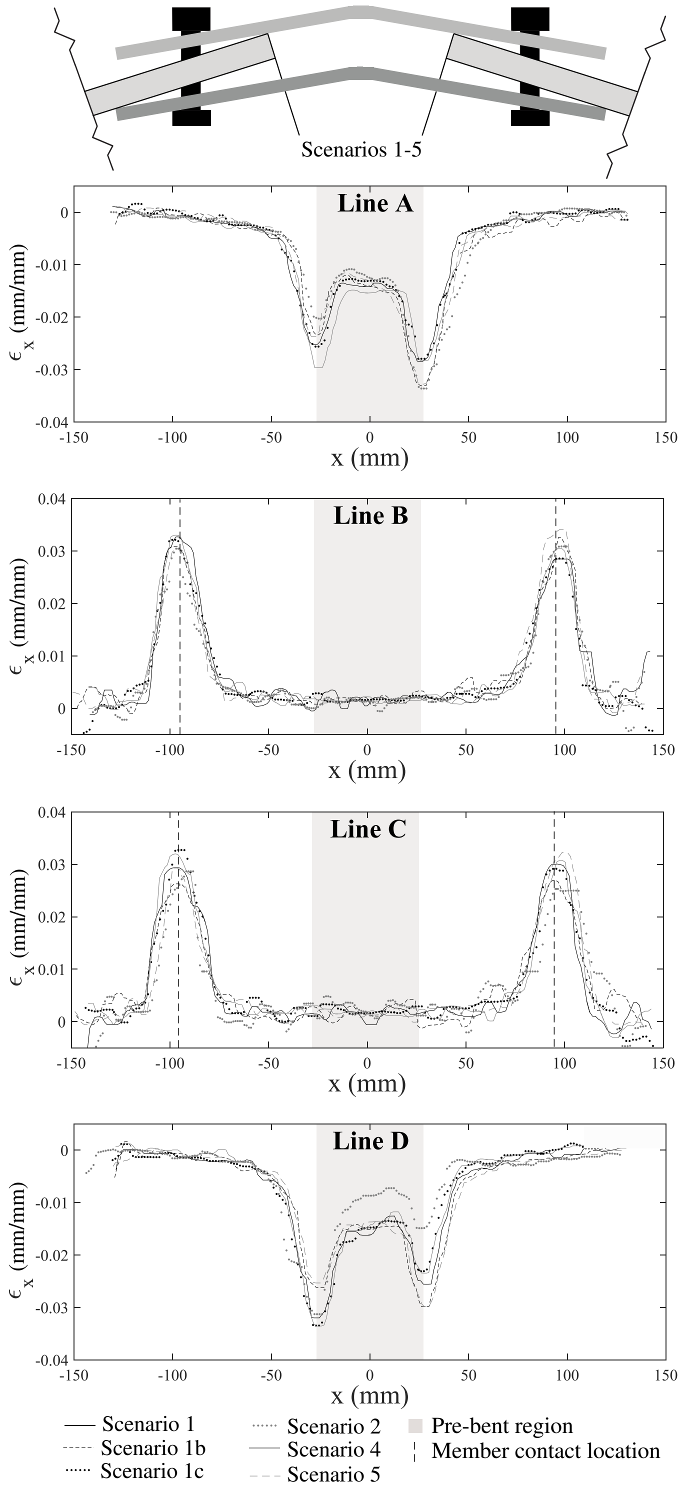

FIG. 8. Effect of bolt tightening procedure: Measured circumferential surface strain (ϵ_x) along lines A-D (Figure 7) for Scenarios 1, 2, 4, and 5 (Table 2).

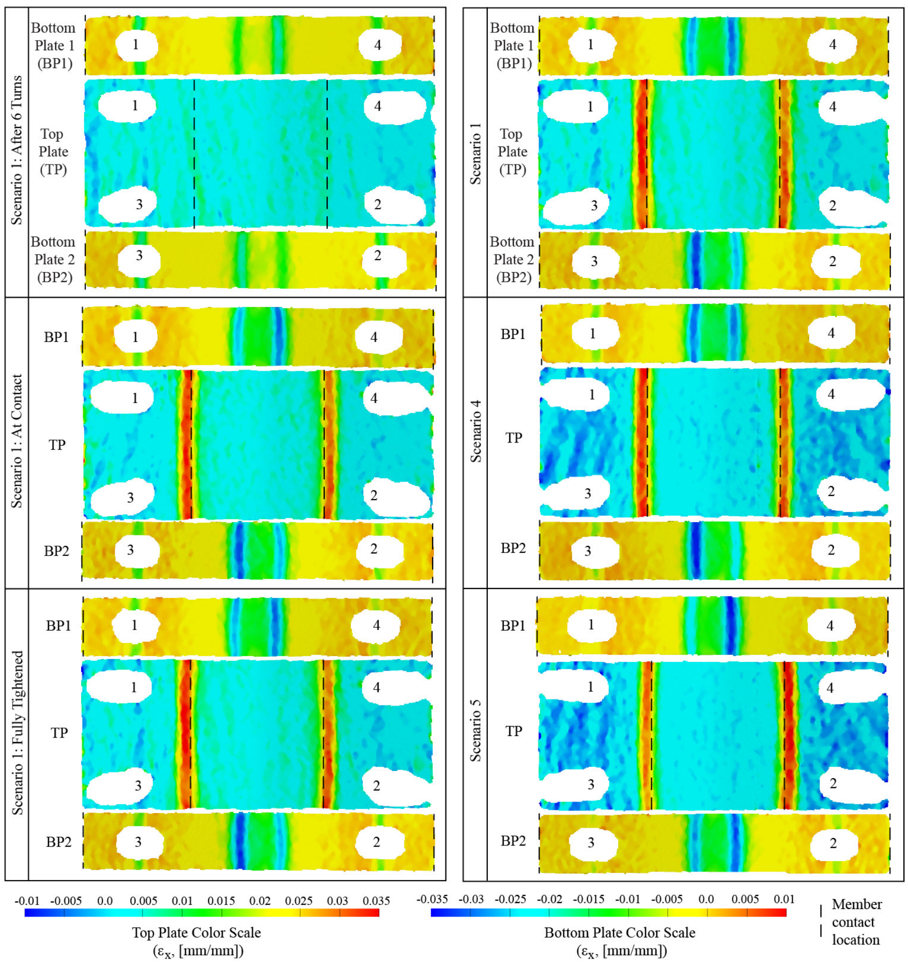

FIG. 9. Effect of bolt tightening procedure: Plan view of measured circumferential surface strain (ϵ_x). The left column indicates the evolution of strains during tightening (Scenario 1). The right column compares tightening patterns (Scenarios 1, 4, and 5, Table 2). All use 1 full turn of each bolt per tightening increment. Numbers indicate bolt identification.

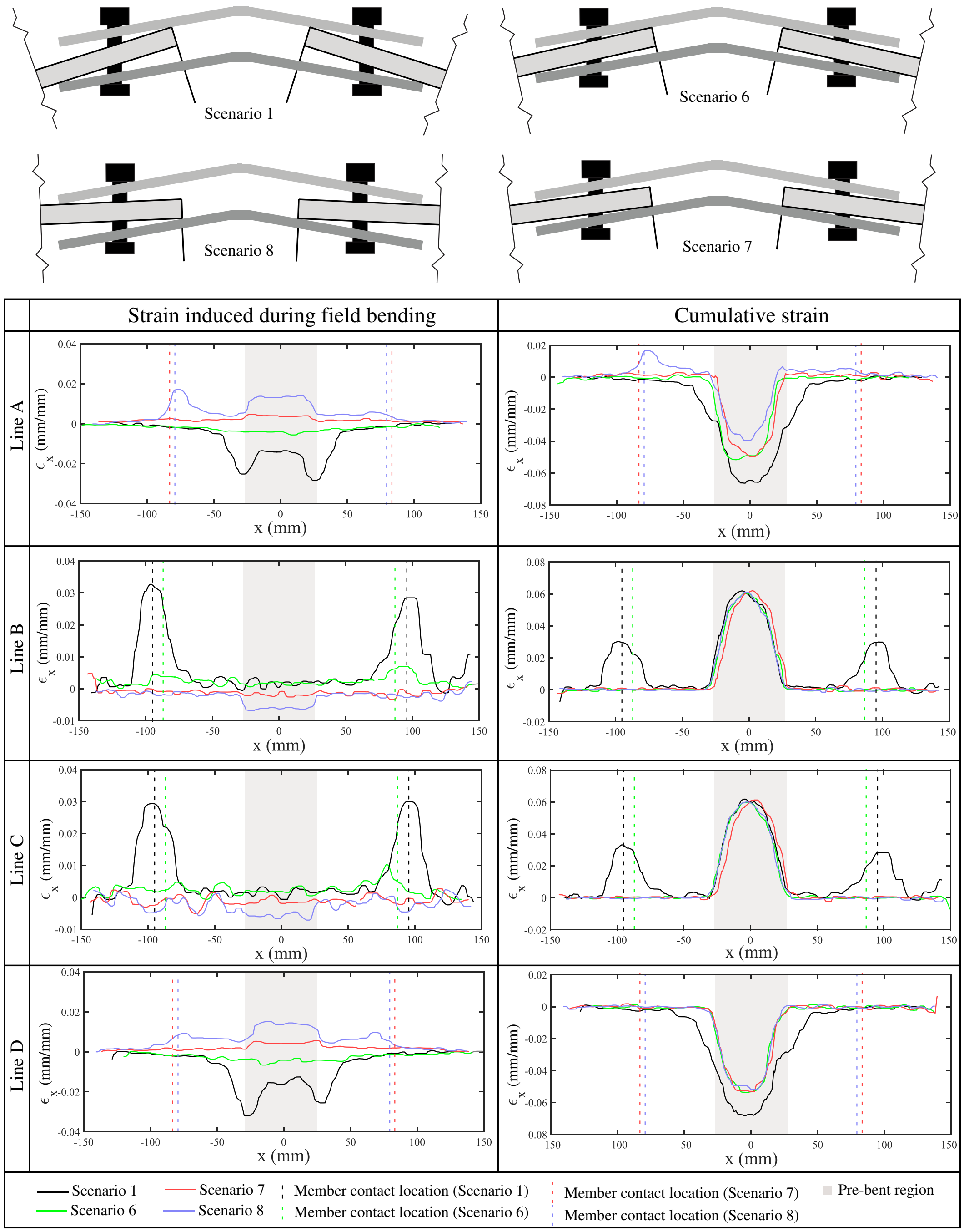

FIG. 10. Effect of amount and direction of bend: Measured circumferential surface strain (ϵ_x) along lines A-D (Figure 7) for Scenarios 1, 6, 7, and 8 (Table 2). The left column indicates strain induced during field bending, the right column shows total cumulative strain from prefabrication and field bending.

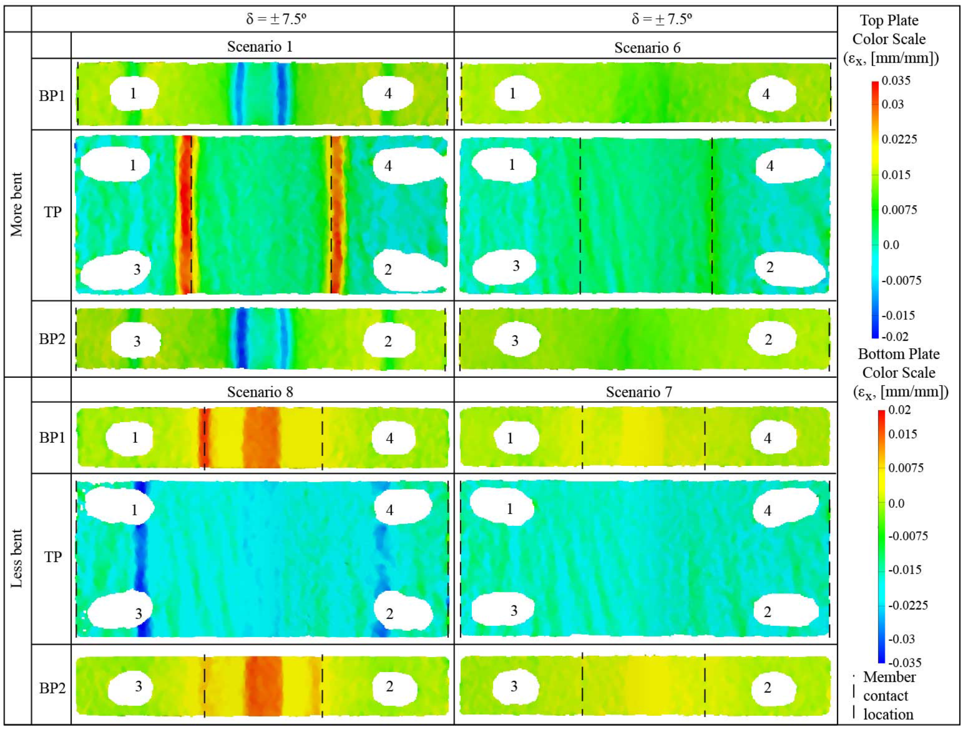

FIG. 11. Effect of amount and direction of bend: Plan view of measured circumferential surface strain (ϵ_x) for Scenarios 1, 6, 7, and 8 (Table 2).

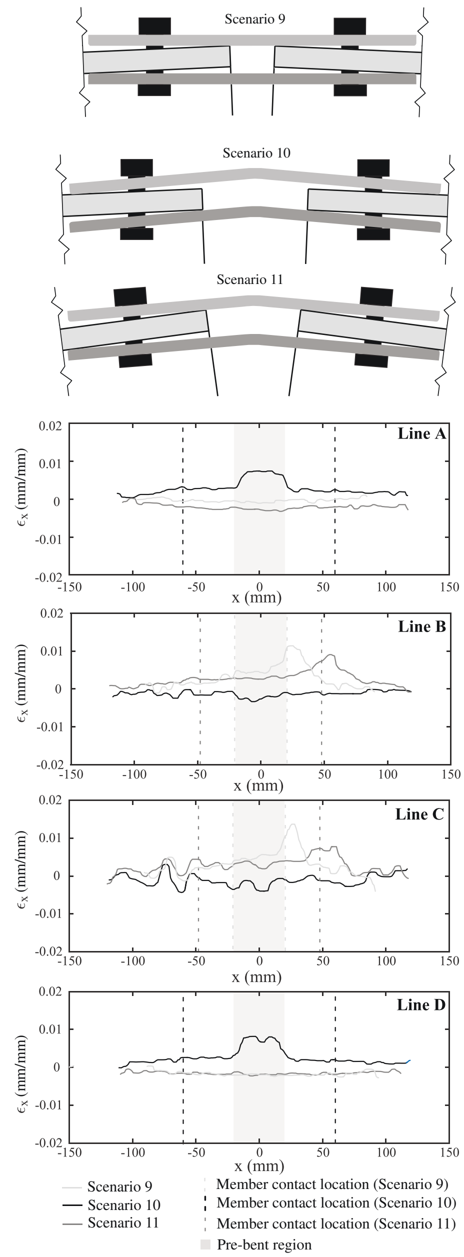

FIG. 12. Effect of varying plate angles: Measured circumferential surface strain (ϵ_x) along lines A-D (Figure 7) for Scenarios 9, 10, and 11 (Table 2).

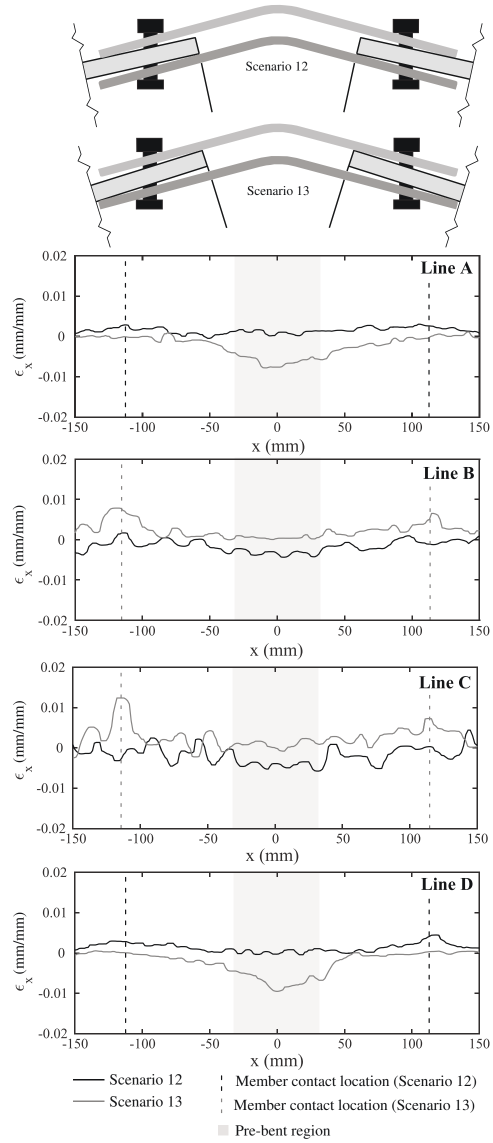

FIG. 13. Effect of varying plate angles: Measured circumferential surface strain (ϵ_x) along lines A-D (Figure 7) for Scenarios 12 and 13 (Table 2).